EPJ Photovoltaics **16**, 4 (2025)

https://doi.org/10.1051/epjpv/2024047

Available online at:
www.epj-pv.org

Special Issue on 'EU PVSEC 2024: State of the Art and Developments in Photovoltaics', edited by Robert Kenny and Gabriele Eder

ORIGINAL ARTICLE OPEN ACCESS

Numerical analysis of evaporation reduction in floating photovoltaic power plants: influence of design parameters

Baptiste Berlioux[1,2,*], Baptiste Amiot[3], Martin Ferrand[3,4], Rémi Le Berre[2], Oume-Lgheit Rhazi[2], Javier Vidal[5], Hervé Pabiou[6], and Ronnie Knikker[1]

[1] INSA-Lyon, CNRS, CETHIL, UMR5008, Villeurbanne 69621, France
[2] EDF R&D, Dpt. Technology and Research for Energy Efficiency, 1 Avenue des Renardières, Écuelles 77250, France
[3] CEREA, Ecole des Ponts, EDF R&D, 9 Rue de la Physique, Marne la Vallée 77455, France
[4] EDF R&D, Dpt. Fluid Mechanics Energy and Environment, 6 Quai Watier, Chatou 78401, France
[5] EDF R&D, Dpt. National Laboratory of Hydraulics and Environment, Chatou 78401, France
[6] CNRS, INSA-Lyon, CETHIL, UMR5008, 69621 Villeurbanne, France

Received: 1 July 2024 / Accepted: 29 November 2024

Abstract. Evaporation reduction is one of the advantages provided by floating photovoltaic (FPV) power plants. However, few studies have yet been carried out to understand how to optimise the layout of FPV power plants in order to provide better water management. Indeed, the interaction between atmospheric conditions, water bodies, and the FPV plant creates a dynamic system that is challenging to study and accurately model. This paper investigates the impact on evaporation of various characteristics of FPV plants, such as float technology, plant positioning and orientation, distribution, and coverage ratio. This study was performed using Computational Fluid Dynamics (CFD) of the surrounding atmosphere, with the impact of the FPV plant modelled using specific boundary conditions to reduce computational costs. The numerical results show that the coverage ratio is the most important factor in reducing evaporation. Full coverage could reduce evaporation by 52.8% for a plant with a large footprint on the water and by 43.4% for a plant with a smaller footprint. Other parameters have only a moderate impact, allowing the fine-tuning of evaporation reduction. The optimal configuration would involve covering the entire water body with a single large water footprint island positioned downwind of the prevailing transversal winds. This setup significantly reduces evaporation, thereby enhancing water conservation and making an FPV power plant a valuable tool in sustainable water management.

Keywords: Floating photovoltaic (FPV) / evaporation reduction / CFD / microclimate / moist air

1 Introduction

In the current environmental context, the need to find greener ways to generate electricity has become a priority. In the face of the climate emergency and the depletion of fossil fuels, it is imperative to turn to renewable and sustainable energy sources. Solar energy, in particular, offers a promising solution. However, conventional solar panel installations often require large land areas, which can contribute to land stress and limit their deployment potential [1,2].

To overcome this constraint, floating photovoltaic (FPV) systems have emerged as an innovative alternative, enabling the installation of solar panels on water bodies, thereby alleviating pressure on land. Since the first installation in Japan in 2007 of 20 p [3], installed capacity has risen sharply, reaching 5.7 p by 2022. And this growth is bound to continue over the coming years. In [4], for example, the increase was estimated at 15% every year for the next 10 years.

The interest in this type of installation is explained by the many advantages it offers. Initially developed to reduce land stress, gains in performance have been observed due to the lower temperature of the modules [2,5,6]. In addition to increasing electricity production, FPV power plant also serves as an effective tool for enhanced water cycle management by potentially reducing evaporation from water bodies. Indeed, the different components of the power plant (panels, floats, structures) partially occlude the surface of the water and limit wind speed, reducing exchanges [7]. As water becomes an increasingly precious

* e-mail: baptiste.berlioux@edf.fr

resource, conservation efforts can prove beneficial, whether for consumption, irrigation, or even hydroelectric power generation, such as the case of coupling floating photovoltaic (FPV) power plants with hydroelectric dams.

Preliminary studies have revealed significant potential for water savings through the use of floating solar panels. For example, Redon-Santafé et al. [8] indicated that for an irrigation reservoir near Alicante, Spain, completely covered with panels (4490), it is possible to save 5000 of water per year. Similarly, Kumar and Kumar [9], using a basic experimental setup, demonstrated that a module can reduce evaporation by 29.1%. With a similar setup, Al-Widyan et al. [10] estimated an evaporation reduction of 31.2% for a 30% covered surface and observed a reduction of 54.5% when 50% of the water surface was covered.

However, these experimental results have several limitations. Firstly, they depend on the specific conditions of the experiments, such as micro-meteorological conditions, reservoir size and methodology, leading to significant variability in the outcomes. Secondly, these studies are often conducted on a small scale, limiting their applicability to larger-scale scenarios. Finally, the experimental parameters are not always clearly defined or controlled, making it challenging to reproduce the results in different contexts.

To address these limitations, other studies have employed various theoretical models to estimate potential water savings. For instance, Lopes et al. [11] estimated the reduction in evaporation for 20% reservoirs in Brazil's semi-arid region. Using the equation developed by Assouline et al. [12] and assuming a uniform evaporation rate proportional to the free water surface, they estimate that 20 coverage of basins reduces evaporation by 13.8%, while 70 coverage reduces it by 55.2%. Finally, Stiubiener et al. [13] indicates that covering an irrigation canal in Brazil with at least 5 of photovoltaic panels could save 25% of the water from evaporation, amounting to 25,000 m^3 per day.

These studies provide a broad estimate that offers a preliminary idea of potential water savings. However, to more accurately estimate the reduction in evaporation on finer time scales, further research is required. Some studies have aimed to provide more precise estimates, considering temporal variations and specific local conditions to refine our understanding of the effectiveness of floating solar panels in reducing evaporation.

For instance, Scavo et al. [14] investigated various types of FPV systems. Using a derived Penman-Monteith model and an empirical model, their findings indicated that systems in direct contact with water can reduce evaporation by 18% to 100% (with, respectively, 10% and 100% of the water surface covered). In contrast, for more aerated systems, the reduction in evaporation is lower, ranging from 6% to 60% for the same coverage rates. Similarly, employing empirical models, Mittal et al. [15,16] estimated that 1 p can save between 20 and 191 million litres of water per year. Rosa-Clot et al. [17], using a model derived from McJannet et al. [18] based on the Penman-Monteith equation, estimated water savings ranging from 15,000 to 25,000 cubic metres per 1 p annually for applications in Southern Australia. Additionally, by comparing different literature models, Santos et al. [19], estimated an evaporation reduction of 60% for a coverage area of 1265 square metres. Other studies have developed more complex models based on energy balances and dynamics above lakes. For example, Kumar and Kumar [9] estimated that a PV module allows an evaporation reduction of 36% for a water tank fully covered by a PV panel. According to Taboada et al. [7], the evaporation reduction is evaluated at 90% when PV panels cover 95% of a pond.

However, these studies mainly rely on empirical models based on various assumptions, such as uniform evaporation rates and simplified interactions between solar panels and water surfaces. Although these models offer a useful starting point, they have limitations, including potential inaccuracies due to overly simple assumptions and an inability to capture the complex dynamics of real-world scenarios. As a result, these empirical approaches may not fully account for factors such as local micrometeorological conditions, surface water temperature and the specific design of floating solar panel systems.

The objective of this study is to assess the effectiveness of FPV power plants in reducing reservoir evaporation using Computational Fluid Dynamics (CFD). Given the limitations of previous approaches, CFD modelling presents a compelling and promising alternative, enabling more detailed and precise simulations of the complex interactions between solar panels, water surfaces, and environmental conditions. By incorporating a diverse set of variables and sophisticated physical models, CFD provides more detailed insight into the mechanisms of evaporation reduction.

Consequently, after analysing the influence of power plant design on evaporation rates, we will explore the impact of atmospheric conditions. This comprehensive approach will help optimise the design and positioning of floating solar panels, leading to more accurate predictions and, ultimately, supporting the large-scale deployment of these systems.

2 Method

2.1 CFD modelling

The microclimate around the FPV array is simulated using the CFD software code_saturne [20]. Based on a finite-volume method, the code_saturne solver allows us to determine the wind velocity, pressure, density, potential temperature, and total water content fields in a control volume, which is presented in the next Section 2.2. A Reynolds average Navier-Stokes (RANS) approach is chosen to compute the mean quantity of the field of interest for each unitary volume in the domain. We are specifically interested in the equation for the specific humidity of air, noted q, which is defined as follows:

$$\partial_t q + \partial_j(u_j q) = \partial_j\left(\mathrm{D_m}\partial_j q - \left(\overline{u_j' q'}\right)\right) \tag{1}$$

where u_j is the velocity in the j direction, $\mathrm{D_m}$ is the mass diffusion coefficient. The last term on the right-hand side is the turbulent diffusion flux which is modelled using a single

gradient diffusion hypothesis which reads $\left(\overline{u_j' q'}\right) = \frac{\nu_t}{Sc_t}\partial_j q$ where ν_t is the turbulent viscosity modelled using a $k-\varepsilon$ turbulence closure and $Sc_t = 0.7$ is the turbulent Schmidt number.

In this work, the geometry of the FPV array is not explicitly represented. Instead, the effect of the FPV array on air flow and water evaporation is modelled using adapted boundary conditions (see Sect. 2.3). Indeed, numerical meshing of the real geometry of a power plant is challenging due to the many small details in the design of modules, frames, and floaters. It is an impractical approach for cases of industrial studies evaluating the effect of several thousands of these obstacles. Modelling the FPV array through adapted boundary conditions reduces computational cost and makes modelling possible at the scale of a real FPV power plant.

The interactions between the surface and the atmosphere for the quantities of interest (momentum, heat, water vapor) are modelled by the Monin-Obukhov Similarity Theory (MOST) [21]. In doing so, the distribution of these quantities in the fully turbulent region above the surfaces is a function of the fluctuation level, the altitude z, and the dynamic surface roughness z_0. For instance, the velocity profile in a neutrally stable atmosphere reads:

$$u(z) = \frac{u^\star}{\kappa}\ln\left(\frac{z}{z_0}\right) \tag{2}$$

where $u^\star$ is the friction velocity at the surface [22], $\kappa = 0.41$ is the von Kármán constant.

2.2 Evaporation process

A multitude of interacting factors influence evaporation so that numerical modelling of the mass transfer can be performed in different manners. Here, it is assumed that there is a thermodynamic equilibrium at the water surface so that the vapour pressure reaches the saturation state $P_{v,s}$, the specific humidity is at the saturated value q_s and the temperature of moist air is equal to that of the water surface, T_w (see Fig. 1). Above the surface, moist air has a humidity q, a temperature T and a vapour pressure P_v. The evaporation flux, i.e. the mass transfer, noted E, is expressed here as follows:

$$E = \beta(q_s - q) \tag{3}$$

with β the convective mass transfer coefficient[1].

According to the MOST, in a neutrally stable atmosphere the evaporation flux in the turbulent region near the water surface can be written as:

$$E = \frac{\rho\kappa u^\star}{\ln\left(\frac{z}{z_0}\right)}(q_s - q(z)). \tag{4}$$

[1] In the literature, other expressions can be found to define this coefficient. For example, the mass transfer can be written in terms of a density or pressure difference as $E = \beta_\rho\,(\rho_s\text{-}\rho)$ or $E = \beta_\rho\,(P_{v,s}\text{-}P)$ with $\beta_\beta = \beta/\rho_h$ and $\beta_p = \beta/(\rho_h\, R_v T)$.

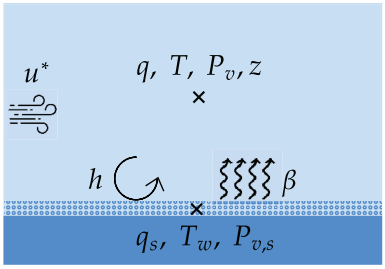

Fig. 1. Diagram of evaporative transfer.

Therefore, the convective mass transfer coefficient β is defined by the relation:

$$\beta = \frac{\rho\kappa u^\star}{\ln\left(\frac{z}{z_0}\right)}. \tag{5}$$

The mass convective transfer rate is dictated by the dynamics of the flow through the friction velocity and by the nature of the surface through the dynamic roughness.

At the water surface, the evaporation flux increases the water vapour fraction of moist air. We assume that the vapour flows from the saturated surface to the turbulent layer at temperature T_w, heat transfer by mass injection can be written as:

$$\begin{aligned}\phi_T &= Ec_{p,v}T_w \\ &= \beta(q_s - q)c_{p,v}T_w\end{aligned} \tag{6}$$

where $c_{p,v}$ is the specific heat capacity of water vapour. To ensure energy balance, this energy rate is injected into the first cell which is the volume of the air just above the FPV array.

In practice, β is calculated directly by the wall functions that describe the profiles of the specific humidity in the fully turbulent zone [23]. However, for the surface covered by an FPV array we define a specific mass transfer coefficient β_{FPV} and a specific roughness length $z_{0_{FPV}}$. These two parameters are calculated using a model previously developed from flow simulations of the entire FPV geometry in the work by Amiot [24]. Since these parameters are sensitive to the design of the module arrangement (pitch, height of the module, tilt angulation) and wind direction, the model includes a set of coefficients taking into account these constraints.

2.3 Boundary conditions

Figure 2 shows the computational domain and the boundary conditions adopted. The bottom of the domain is divided into 3 distinct rough walls : the ground, the lake, and the FPV island. These zones are critical regions in the simulation because of their interaction with the fluid flow.

First, the ground zone represents the land surrounding the lake where a constant dynamic roughness length $z_{0_g} = 0.01$ is established. It mimics a sparsely vegetated area. Moisture and heat fluxes, noted respectively Φ_E and Φ_T, are set to zero to avoid influencing the moisture and heat scalars above the lake surface.

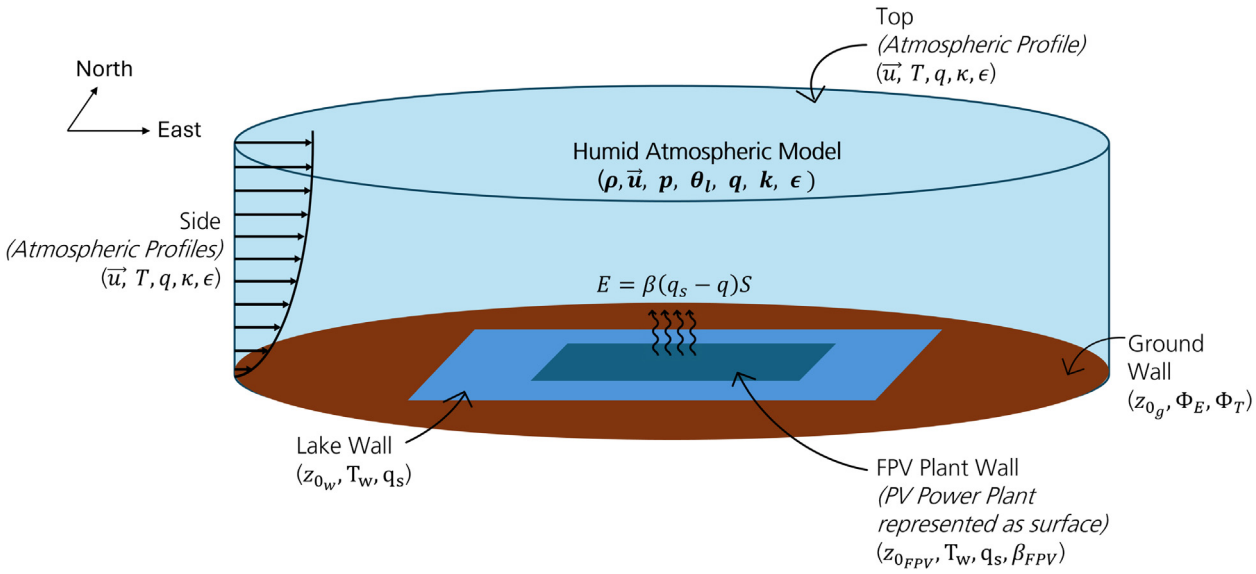

Fig. 2. Computational domain and boundary conditions.

On the uncovered area of the lake, temperature and humidity are imposed at the water temperature and saturated humidity, respectively. The water temperature at the surface is arbitrarily set at $T_w = 290$, allowing us to calculate the corresponding saturated humidity using the equation proposed by Glanz [25]:

$$q_s = 1.35 \times 10^5 \times \exp\left(-\frac{4157}{T_w - 33.91}\right). \tag{7}$$

The water surface is modelled as a rough wall, and, accordingly the lake roughness length z_{0_w} is estimated from [26]:

$$z_{0_w} = 1.2 \times 10^{-2} \times \frac{u^{\star 2}}{g_z}. \tag{8}$$

For the FPV area, in addition to T_w and q_s, the convective mass transfer coefficient β_{FPV} and the roughness length denoted $z_{0_{FPV}}$ are imposed. These two parameters represent the impact of the FPV array on the moisture exchange and the flow dynamics (see Sect. 2.2). Therefore, the mass transfer is modelled by equation (3) with $\beta = \beta_{FPV}$.

For the remaining boundaries of the domain (the sides and the top), Dirichlet conditions are applied for velocity, liquid potential temperature, and humidity. The velocity follows a logarithmic profile which corresponds to neutral atmospheric conditions as described by the MOST. This means that the wind speed increases logarithmically with height above the ground, reflecting the typical behaviour of wind in a neutral atmosphere (see Eq. (2)). In practice the velocity at 10m is given which allows to find the friction velocity u_*. Both the liquid potential temperature and the humidity are set to be constant with altitude. This implies that there are no vertical gradients in these quantities, simplifying the boundary conditions and maintaining consistency with the neutral atmosphere assumption.

2.4 Evaporation reduction

In the presence of wind, convective mass transfer is a key parameter driving evaporation. Therefore, the presence of an FPV array above the water body is expected to reduce evaporation as it reduces the mean air velocity in the vicinity of the surface as well as the exposed water surface.

However, there are currently too many possible FPV power plant designs – including the type of float, the location on the reservoir, the number of PV islands, their shape, orientation, and coverage rate – and too few design guidelines specifically oriented towards reducing evaporation. Therefore, to identify those with the most significant impact on evaporation reduction, the following parameter ε_{evap} is defined:

$$\varepsilon_{evap} = \frac{E_{open} - E_{PV}}{E_{open}}. \tag{9}$$

E_{open} represents the evaporation of the open water body, while E_{PV} corresponds to the evaporation of the water body partially covered by PV panels.

It seems quite evident that the area occupied by the FPV plant is a key parameter in reducing evaporation. Three parameters can be defined to describe plant coverage: the Overall Coverage Ratio (OCR), the Ground Coverage Ratio (GCR), and the Water Coverage Ratio (WCR) which are defined by:

$$OCR = \frac{S_{FPV}}{S_{Lake}} \tag{10}$$

$$GCR = \frac{S_{PV_T}}{S_{FPV}} \tag{11}$$

$$WCR = \frac{S_{w_T}}{S_{FPV}}. \tag{12}$$

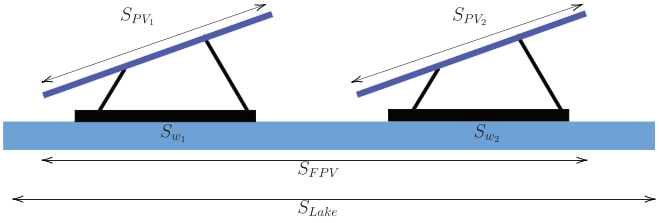

Fig. 3. FPV characteristics.

Fig. 4. Reference case.

As illustrated in Figure 3, S_{Lake} represents the total surface area of the lake, while S_{FPV} denotes the total projected surface area of the FPV plant including inter-row and column space. S_{PV_T} is the effective PV panel surface of the plant. S_{w_T} refers to the surface area of the plant in direct contact with the water, primarily the area covered by the floats.

2.5 Case studies

The simulations are carried out for a circular domain with a diameter of 1500 m and a height of 40 m, discretized using 2,14,000 hexahedrons. The simulations run over 100 s with a time step of 0.1 s, which is sufficient to obtain a steady state given constant boundary conditions (Sect. 3.1). The Courant—Friedrichs–Lewy (CFL) condition is respected throughout the simulation, ensuring numerical stability with CFL values remaining below 1. The case study used as a reference shown in Figure 4, consists of a single square island placed at the centre of the reservoir, which is also square. Initially, the *OCR* is set to 50%. The wind blows constantly from west to east at a speed of 5.9, measured at a height of 10m. The airflow enters in the domain at a temperature of 290k with a specific humidity of 0.0031kg–1 ($RH = 26\%$). At ground level, the pressure is 1000 hPa, and the water temperature is also set at 290 K.

The parameters β_{FPV} and z_{FPV} (see Sect. 2.3) are defined for specific PV array arrangement. A wide range of floats are currently available on the market. These can be broadly classified with respect to the float's surface in contact with water. *WCR* serves as a key indicator of the FPV power plant footprint on the water. In this study, two installations are compared: type *I* floats, characterized by a large surface area in direct contact with the water, with a *WCR* of 60% (see Fig. 5a), and type *II* floats, which have a much smaller contact area, with a *WCR* of only 10% (see Fig. 5b). For float type *I*, PV panels are oriented in landscape with a 12° tilt angle. The spacing between rows and columns is set to achieve a *GCR* of 80%. In contrast *II*, panels are in portrait format with a 25°. The *GCR* is set at 90%.

3 Results

Sensitivity studies are conducted in order to better understand the impact of FPV power plants on water reservoirs on the evaporation rate. Successively, after a comparative study of two float design, the effects of plant positioning, the number of islands, orientation relative to wind direction, coverage ratio and atmospheric conditions on the reduction of evaporation are assessed.

3.1 Float design comparison

Figure 6 shows the evolution of the evaporation rate for the two configurations during 100s, sufficient to reach the steady state. For the case without coverage (open water), the global evaporation rate of the reservoir is 0.52 at mm h–1 steady state. For the coverage cases, the global evaporation rate of the reservoir is 0.38 mm h–1 for the type *I* configuration and 0.41 mm h–1 for the type *II* configuration. This corresponds to global evaporation reductions of 26.5% and 21.4%, respectively.

As expected, the configuration with the larger water footprint on the reservoir ($WCR = 60\%$) results in lower reservoir evaporation. However, the impact of the water footprint is low despite the large difference in *WCR* for the two types of floats. Evaporation rate is the product of the mass transfer coefficient β and the specific humidity difference $q_s - q$ above the surface (Eq. (3)). Figure 7 presents the evaporation rate, specific humidity difference and mass transfer coefficient at the interface at steady state along the centre line of the FPV plant parallel to the wind speed for the three configurations. The presence of the FPV array tends to reduce the mass transfer coefficient while increasing the specific humidity gradient. However, the mass transfer coefficient is lower for configuration *I* while the humidity difference is larger, compared to configuration *II*. This explains why the difference in evaporation rates between the two configurations remains small despite the differences in footprint.

Additionally, as expected, the reduction in evaporation is significant at the plant zone (indicated by the gray area in Fig. 7). In this area, a reduction of 52.9% for type *I* and 43.6% for type *II* is observed.

Downwind of the FPV, in the open water zone (located to the right of the shaded area in Fig. 7), a slight increase of evaporation is observed. Indeed, the presence of the power plant induces increased turbulence in the airflow, which results in a significant enhancement of the exchange processes between the water and the atmosphere at its outlet [27]. Accordingly, an increase in the β mass transfer coefficient is noted in Figure 7, exceeding the values observed in the absence of the power plant (see Eq. (5)). Progressively, the turbulence level returns to normal, reducing exchanges and thus evaporation. Therefore, at the end of the lake, few difference is observed between the configurations without and with PV coverage.

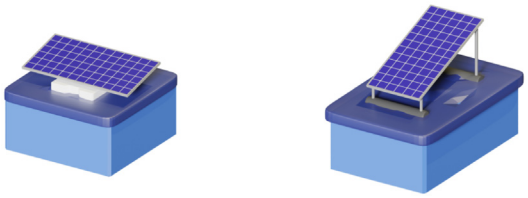

(a) Type I (b) Type II

Fig. 5. Configuration comparison.

3.2 Location of the FPV power plant on the water body

The position of the FPV plant on the reservoir is now investigated. In addition to the centred position (C), four new positions are studied: North (N), South (S), West (W) and East (E) of the lake (cf. Fig. 8). In each case, the same overall coverage ratio is maintained ($OCR = 50\%$).

The corresponding steady-state evaporation reductions are shown in Figure 9. The position of the FPV power plant seems to have only a slight influence on the overall evaporation of the reservoir, leading to a constant reduction of 26.5% for configuration *I* and 21.4% for configuration *II*.

Only minor variations in water gains are observed between the five positions exposed. As shown by Figure 10, these minor differences are due to the positioning of the power plant on the reservoir in relation to the west-to-east orientated wind (see Sect. 2.5). By positioning the PV island to the east, the free water zone at the power plant outlet is reduced, avoiding increased evaporation due to higher turbulence as described in Section 3.1. Conversely, when the PV island is positioned to the west. However, as shown by Figure 9, the real impact remains very limited, increasing or reducing the reduction in evaporation by around 0.2%, which is negligible.

Furthermore, for the same reasons, as shown in Figure 9, positioning the PV plant to the north, south, or in the middle of the reservoir while maintaining the same fetch (distance from the shore relative to the dominant and constant west-to-east wind) does not alter the total evaporation from the reservoir. The plant acts as a uniform obstacle regardless of its location along the shoreline, thus maintaining similar conditions for evaporation at different positions.

3.3 Number of PV islands

Maintaining the same overall coverage rate ($OCR = 50\%$), the main island is successively subdivided into 4, 9 and 16 square sub-islands, evenly distributed across the reservoir (see Fig. 11).

As depicted in Figure 12, dividing the plant into islands shows minimal influence on evaporation. There is a marginal decrease in evaporation reduction for configuration type *I*. The evaporation reduction changes from 26.5% with a single island to 26.4% with 16 islands. For configuration type *II*, the decrease is slightly greater, from 21.4% to 21.0%.

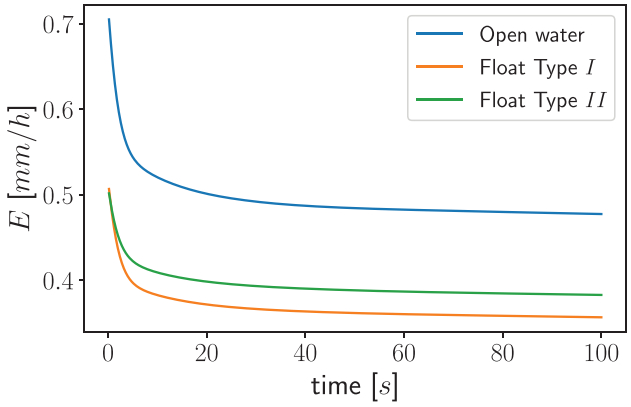

Fig. 6. Time evolution of the evaporation rate: simulations are run for 100 seconds to reach steady state.

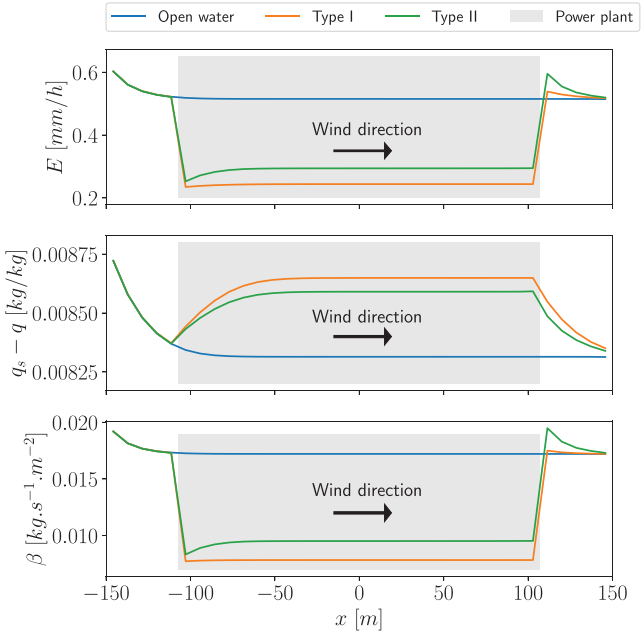

Fig. 7. Evaporation rate (E), specific humidity difference (q_s–q) and mass transfer coefficient (β) profiles along the water reservoir. Grayed area corresponds the size of the FPV plant.

These marginal differences are attributable to the same reasons explained previously (see Sects. 3.1 and 3.2). Depending on the extent of the free water zone downstream of the islands, the evaporation of this zone is increased.

These findings are noteworthy for practical applications. In real-world scenarios, particularly in cases where the geometry of a lake or reservoir makes it challenging to deploy a large, single island, subdividing the plant into smaller islands may be necessary. It may also facilitate deployment and maintenance. What is particularly encouraging is that despite this subdivision, the overall effectiveness of the plant in reducing evaporation remains unchanged.

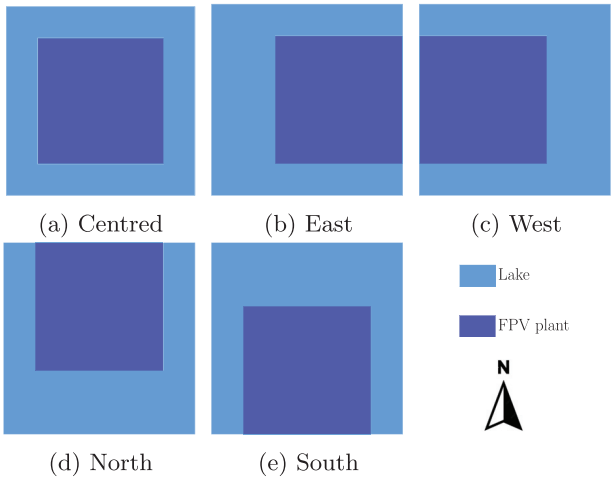

Fig. 8. Different positions of the PV plant investigated in this study.

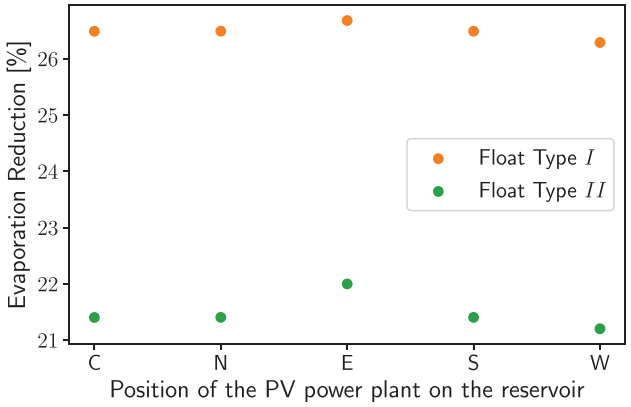

Fig. 9. Evaporation Reduction (ε_{evap}) of the water reservoir for 5 different PV plant position.

While these conclusions are promising, it is important to acknowledge the limitations of this case study. The study assumes an idealized, square-shaped lake with evenly distributed square sub-islands and constant wind blowing from a single direction. These simplifications may not fully capture the complexity of real-world reservoirs, which can have irregular shapes, varying wind directions. Additionally, the square sub-islands used in this study may not represent the optimal geometry for every environment, particularly in cases where the wind direction shifts or where islands of different shapes and orientations could have a more pronounced effect on evaporation.

To address this, the next phase of the study investigates how wind directions influence the effectiveness of FPV arrays in reducing evaporation.

3.4 Power plant orientation relative to wind direction

Here, the impact of plant orientation on evaporation is analysed for configuration *I*. For this numerical experiment, the plant is relocated to the centre of the lake and a constant *OCR* of 50 is maintained. The PV modules are south-oriented in order to mimic a real installation that

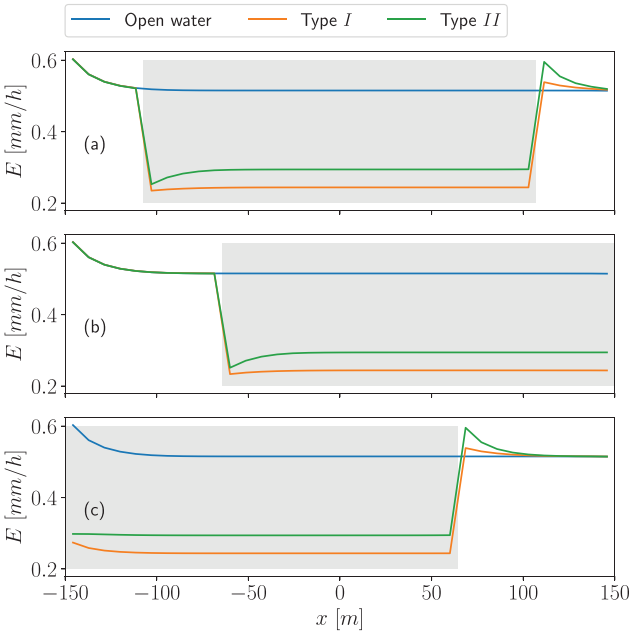

Fig. 10. Evaporation rate (E) profiles along the water reservoir for power plants located on the centre (a), east (b) and west (c) of the water body. Grayed area corresponds the size of the FPV plant.

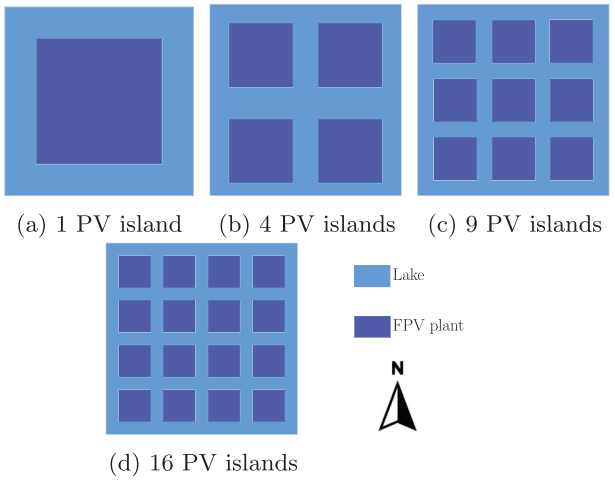

Fig. 11. PV islands distribution on the reservoir.

attempts to maximise electrical production (northern hemisphere). We study seven wind directions, making angles of 0°, 5°, 10°, 45°, 90°, 135° and 180° relative to the north (0°). When the wind comes from north (0°), the wind reaches the back of the panels first. These wind conditions are called tailwinds hereafter. Conversely, when the wind comes from the south (180°), the wind hits the front of the panels first. These conditions are called headwinds. Note that winds from the east or west directions blow the panels from the side and such conditions are called crosswinds in the following. Due to the symmetry of the study case, crosswinds from east and west give the same results.

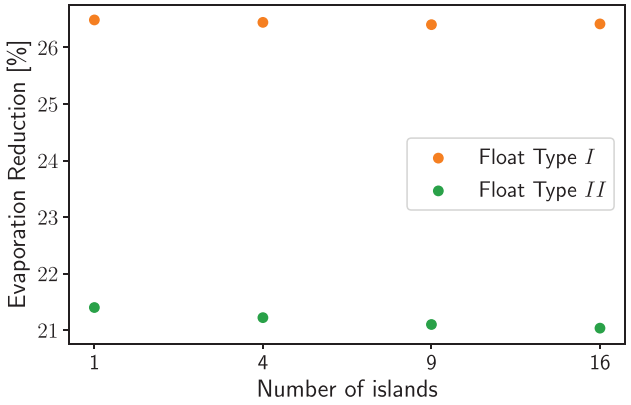

Fig. 12. Evaporation reduction (ε_{evap}) of the water reservoir for different numbers of islands.

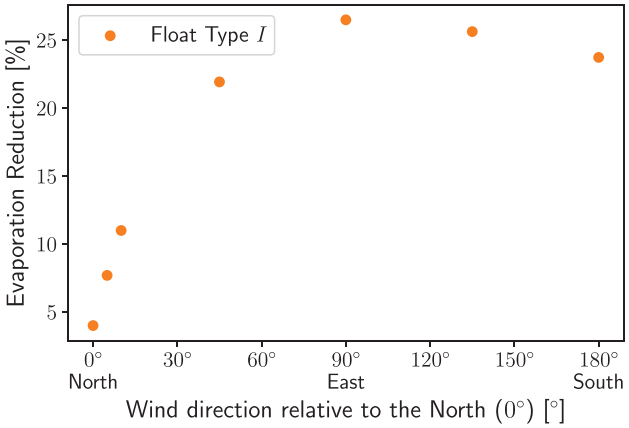

Fig. 13. Evaporation reduction (ε_{evap}) of the water reservoir for different wind directions relative to the north (0°).

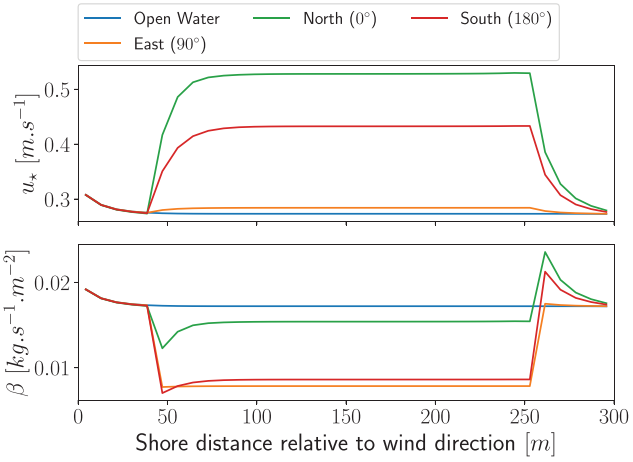

Fig. 14. Friction velocity u^* and mass transfer coefficient β profiles for north, south and east wind direction relative to the north (0°).

Figure 13 shows the evaporation reduction (see equation (9)) for the seven wind directions of interest. Since, by construction, the evaporation from the uncovered waterbody is not affected by wind direction, the evolution of evaporation reduction as a function of wind direction is due only to the plant orientation with respect to the wind directions (PV orientation versus wind direction). It can be seen that tailwinds (0°) lead to a minimal evaporation reduction of only 4.0% whereas crosswinds produce the largest evaporation reduction (26.5%). The southerly winds are slightly less effective, with an evaporation reduction of 23.7%. These variations can be explained by the various effects of turbulence that are not constant as the wind direction evolves. For tailwinds, the turbulence increases significantly due to the shape of the floating panels, causing the wind to be redirected from the top of the module to the bottom, which allows more airflow beneath the panels. This added turbulence increases evaporation rate and therefore limits the evaporation reduction. Conversely, with headwinds (south direction), the power plant acts as a barrier for the airflow: the front face of the panels deflects the wind upward, reducing the wind speed beneath the panels, thereby diminishing exchanges and so increasing evaporation reduction. As demonstrated in Figure 14, crosswinds (in orange) generate the lowest turbulence levels (measured by friction velocity), nearly matching those of the uncovered waterbody. Given this similarity, one might expect the evaporation rates to be comparable. However, the FPV plant effectively covers a part of the waterbody, significantly limiting the evaporation process, as indicated by the minimal β (in orange) values in Figure 14. With reduced turbulence, the "efficiency" of the plant in blocking evaporation is enhanced, leading to a greater reduction compared to other wind directions.

3.5 Coverage ratio

From the analysis of the various parameters that affect evaporation from photovoltaic installations on water bodies, it appears that most of these parameters have a relatively modest effect. Furthermore, design choices such as the type of float, the position, the number of islands, and the orientation are often constrained by the natural characteristics of the site. As is shown hereafter, the most important parameter that influences evaporation is the coverage rate. By adjusting the percentage of surface covered by the FPV plant, it becomes evident that the overall evaporation of the reservoir can be more or less limited.

Simulations are performed for 7 different overall coverage ratios. The first is the open water reference case with a coverage rate of 0, which is then compared to the following PV coverage ratios: 10%, 25%, 50%, 70%, 90% and 100% (cf. Fig. 15).

As expected and illustrated in Figure 16, higher coverage ratios lead to less evaporation of the reservoir. A larger PV plant effectively reduces evaporation over a more extensive area. For instance, with the plant covering only 10 of the reservoir, evaporation is reduced by 5.1% for configuration I and 4.0% for configuration II. When the plant covers the entire reservoir (OCR= 100%), configuration I achieves an evaporation reduction of 52.8%, while

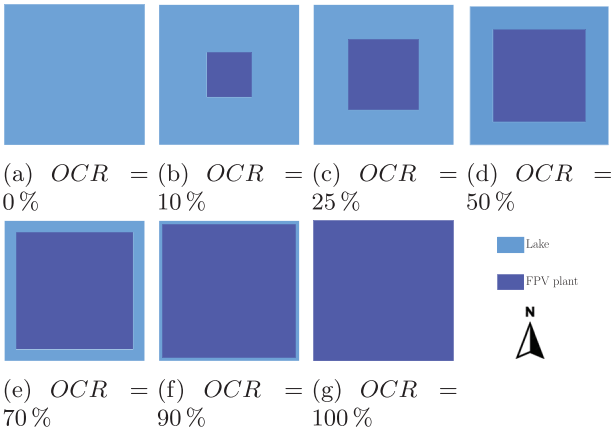

Fig. 15. Illustration of coverage ratio *OCR* of PV island.

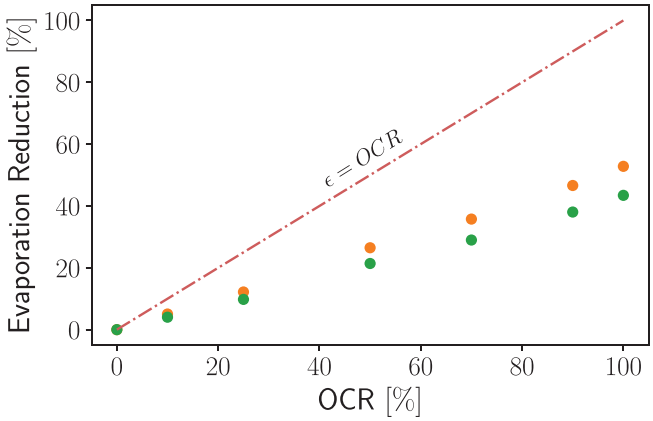

Fig. 16. Evaporation reduction (ε_{evap}) of the water reservoir for different PV plant overall coverage ratios *OCR*.

configuration *II* reduces evaporation by 43.4%. At high coverage ratios, configuration *I* shows a higher reduction of evaporation compared to configuration *II*. With *OCR* set at 10%, the difference between the two configurations is only 1.0%, which is minimal. When $OCR = 100\%$, configuration I is 9.4% more effective than configuration *II*.

Moreover, as we can see, thanks to the red line in Figure 16, the evaporation reductions of the two configurations are not strictly proportional to the coverage ratio, specially for high coverage ratio. However, the evaporation reduction remains fairly linear in relation to the *OCR*. From our findings, the reduction can be roughly approximated as: $\varepsilon_{evap} = \alpha \times OCR$, with $\alpha = 0.58$ for configuration *I* and $\alpha = 0.43$ for configuration *II*. This relationship helps optimise the design of FPV plants to maximise evaporation reduction.

3.6 Sensitivity to atmospheric conditions

The evaporation rate is significantly influenced by local climatic conditions. Above studies were conducted under constant atmospheric conditions, which limits their applicability to varying environments. To address this limitation, sensitivity analyses are performed with respect to the different atmospheric conditions, focusing on the effects of wind speed, ambient humidity, and water temperature. In each analysis, the variable of interest is varied while all other parameters are kept constant. In Figures 17 and 18, the vertical red lines correspond to the reference conditions used in the previous sections.

The atmospheric conditions used in these sensitivity studies may not always reflect real-world scenarios, such as a relative humidity set at 100%. The objective here is to understand the individual influence of each parameter, and by isolating and varying only one parameter at a time, we can verify the model's response to specific changes and ensure its robustness under general conditions.

As illustrated in Figure 17, evaporation rates are significantly influenced by wind speed, ambient humidity and water temperature. Higher wind speeds enhance the exchange of water vapour between water surface and air, thereby promoting higher evaporation rates (see Fig. 17a and Eq. (3)). In Figure 17b it is seen that when ambient humidity reaches saturation (i.e., 100% relative humidity), evaporation is reduced to zero since the air can no longer accommodate additional water vapour, effectively reducing the humidity gradient at the water surface to zero (Eq. (3)). By increasing the water temperature, the saturation humidity at the reservoir surface also rises (see Eq. (7)). As a result, the air humidity gradient at the water surface becomes steeper, thereby increasing evaporation (see Fig. 17c and Eq. (3)).

However, as shown in Figures 18b and 18c the reduction in evaporation remains constant across varying levels of relative humidity and water temperature for both configurations. This indicates that the evaporation rate of the covered waterbody is proportional to that of the uncovered waterbody (see Eq. (9)). This stability can be attributed to the fact that variations in relative humidity and water temperature primarily influence the difference in specific humidity in equation (3), affecting both covered and uncovered areas similarly.

In contrast, a sensitivity analysis of wind velocity reveals that evaporation reduction is more responsive to changes in wind speed (see Fig. 18a). The evaporation reduction tends to decrease as wind speed increases with a more pronounced decline observed at lower wind speeds. For instance, in configuration *I*, when U_{10} is $0.81\,\mathrm{m\,s^{-1}}$, evaporation reduction is estimated at 30.6%, but this drops to 25.5% when U_{10} reaches $9.8\,\mathrm{m\,s^{-1}}$. This behaviour underscore the direct influence of wind speed on the mass transfer coefficient. The effect varies between the uncovered waterbody, where β is given by equation (5), and for the covered waterbody where β_{FPV} is derived from a detailed model, as explained in Section 2.2. Consequently, the mass transfer coefficient does not increase uniformly between open and covered reservoirs as shown in Figure 19. This explains the influence of velocity on the reduction in evaporation, as seen in Figure 18a.

Moreover, at wind speeds $U_{10} \approx 5.9\,\mathrm{m\,s^{-1}}$ a typical value for wind at 10 meters in the atmosphere–the influence of wind speed on evaporation reduction starts to level off.

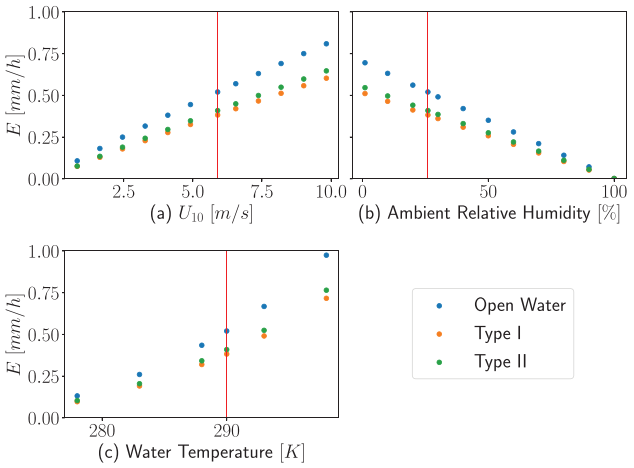

Fig. 17. Water reservoir evaporation for different wind velocities (a), ambient relative humidities (b) and water temperatures (c). Vertical red lines represent reference conditions.

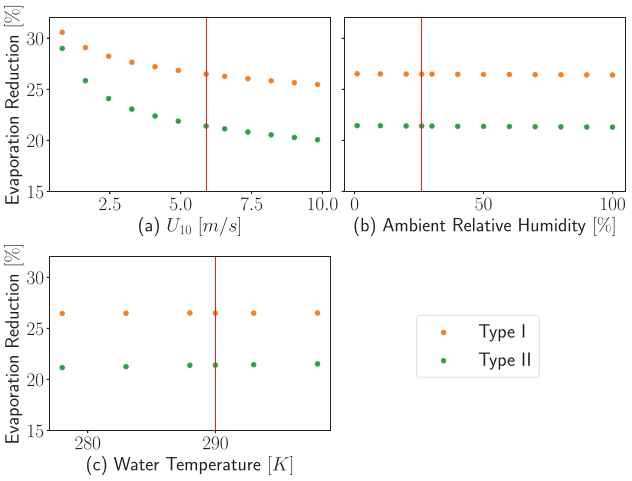

Fig. 18. Evaporation reduction of water reservoir evaporation for different wind velocities (a), ambient relative humidities (b), and water temperatures (c). Vertical red line represents reference conditions.

Despite wind speed increasing by a factor of 1.6, the reduction in evaporation decreases only slightly from 26.5% to 25.5%.

These findings suggest that although atmospheric factors like wind speed, humidity, and temperature do influence evaporation, their impact on evaporation reduction is nil or relatively limited. The primary factor determining the effectiveness of an FPV plant in reducing evaporation remains the system's design, particularly the coverage rate (see Sect. 3.5). This emphasises the importance of optimising coverage to maximise the plant's ability to mitigate evaporation.

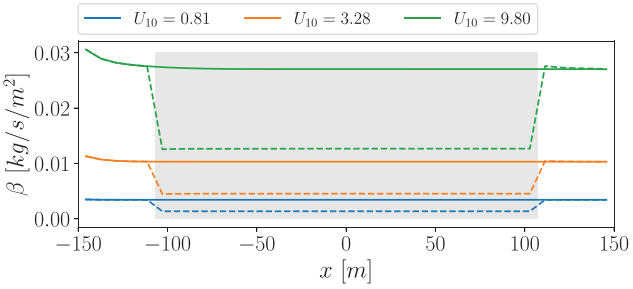

Fig. 19. Configuration I – Mass transfer coefficient β profiles along the water reservoir without (–) and with (– –) coverage for three different wind velocities.

4 Discussion

The objective of this study is to propose a novel methodology for estimating evaporation reduction achievable by any FPV power plant, taking into account its design and the prevailing atmospheric conditions. These sensitivity studies, particularly innovative at the scale of large power plants, provide a comprehensive evaluation of how various design parameters influence the evaporation reduction performance of FPV systems. By systematically examining factors such as float design, plant orientation, and coverage ratios, our research aims to identify optimal configurations that conserves as much water as possible while accounting for the specific characteristics of local environmental conditions.

However, it is important to note that this methodology is entirely numerical, and the results have not been validated with experimental data. The approach relies on CFD simulations, which, despite inherent assumptions, offer a physics-based framework capable of capturing the complex processes driving evaporation.

The current model incorporates several simplifying assumptions of varying importance. For instance, the lake and FPV plant geometries in this study are idealized as square-shaped, which is not representative of most real-world reservoirs or floating installations. Actual reservoir shapes are often irregular, and real FPV plants can take on much more complex configurations, both of which could affect airflow, turbulence, and evaporation rates. Also, boundary conditions are assumed constant. While this may seem a coarse approximation, it allows us to isolate and assess the influence of different parameters on evaporation and its reduction. In particular, for wind direction, a more refined approach could involve analysing wind roses and aggregating wind direction data statistically to estimate percentile-based evaporation reductions. Additionally, the model assumes uniform water temperature across the reservoir, including beneath the FPV plant. This is a strong assumption, as one might expect temperature variations under the plant due to changes in thermal dynamics and solar radiation. However, existing studies do not provide conclusive evidence on this matter. While some influence has been observed, it appears to be minor. For instance, Ilgen et al. [28] reported a maximum surface temperature reduction of −2.4 °C beneath the FPV system, whereas in other cases, FPV installations slightly increased water temperatures at night, with a maximum difference of +1.4 °C. The observed temperature differences rarely exceed 3 °C, suggesting that our assumption is adequate for capturing the first-order drivers of evaporation for the entire waterbody. Moreover, as

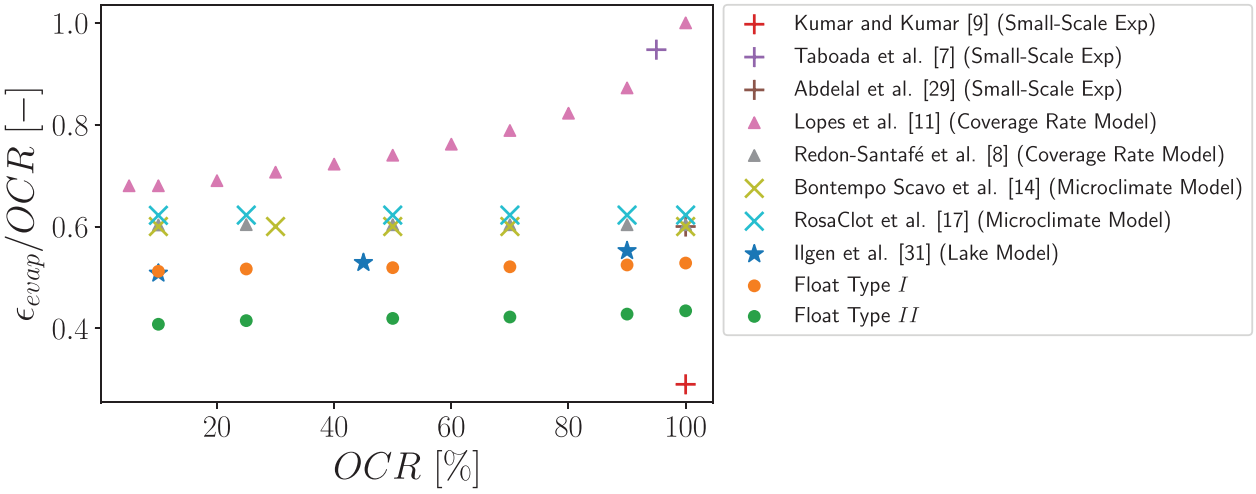

Fig. 20. Comparison of evaporation reduction (ε_{evap}) with literature results.

demonstrated by our sensitivity study on water temperature, variations in this variable do not significantly influence evaporation reduction.

Despite these simplifications, the assumptions allow for consistent comparison between the three configurations studied (Open Water, Type *I*, and Type *II*). Future improvements could include integrating a lake model to better account for the plant's effects on the water body, as well as considering the influence of land and shoreline interactions more thoroughly.

To further validate the numerical model, Figure 20 shows the comparison of our results with those in the literature. To the best of our knowledge, accurately measuring evaporation on the scale of an FPV power plant is inherently complex and has not yet been achieved. Existing studies are mostly limited to small-scale laboratory experiments using water tanks, which are prone to boundary effects that may compromise the applicability of the results to the scale of a whole plant [7,9,29]. As illustrated by the horizontal cross points (+) in Figure 20, these experiments often involve only a single coverage rate and specific designs, resulting in varied outcomes even under similar conditions. Nonetheless, the evaporation reduction reported by Abdelal et al. [29] is in agreement with our findings.

In Figure 20, we also compare our results with analytical models (represented by triangle points △), which account only for the effect of coverage ratio [8,11]. For instance, the estimates from Redon-Santafe [8] are similar to our configuration *I*, as both involve floats with a significant footprint on the water. At full coverage ($OCR = 90\%$), their model overestimates our evaporation reduction by only 7.5%. On the other hand, larger differences are observed in the estimates from Lopes et al. [11], especially at high coverage ratios, where their model assumes that FPV plants act as perfect covers that completely prevent evaporation. More sophisticated models, represented by cross points (×), take into account variables such as wind speed, radiation, and humidity [14,17], resulting in stronger agreement between their estimates and ours. For example, for systems partially in direct contact with water, our model differs by 7% (configuration *I*) from the predictions of Bontempo Scavo et al. with an *OCR* of 100%.

Using the General Lake Model [30], represented by star points in Figure 20, Ilgen et al. [31] predicted a 49.7% evaporation reduction at an *OCR* of 90%, which closely matches our result of 46.6%. It is important to notice that, except for two studies based on small-scale laboratory experiments, the evaporation reduction given by our CFD-based simulation align with most of the existing studies. In particular, it shows that the evaporation reduction is, in a rough estimation, proportional to the overall coverage ratio.

Finally, we observe that as the models become more sophisticated – incorporating variables such as wind speed, radiation, and humidity – their predictions align more closely with our CFD-based simulations. This trend underscores the value of using CFD, as it captures the detailed physical processes that simpler analytical models often miss. The CFD approach allows us to refine predictions and account for the complex interactions between environmental factors and the power plant's design, ultimately leading to more accurate estimates of evaporation reduction. Thus, the importance of CFD in this context becomes evident, offering a powerful tool for both design optimisation and performance evaluation of FPV systems.

5 Conclusions

In conclusion, this numerical study, using advanced CFD simulations, provides critical insights into the key factors driving evaporation reduction in FPV power plants. The results highlight that maximum water savings can be achieved by maximizing reservoir coverage with a large FPV island that has a significant water footprint. Placing the FPV island along the reservoir's maximum fetch and

orienting it to allow prevailing winds to cross the plant further optimises evaporation reduction. Under these optimal conditions, evaporation reduction is estimated at 52.8% for configuration *I* and 43.4% for configuration *II*.

In practice, only design parameters can be oriented toward reduce evaporation. The overall coverage ratio (OCR) emerges as the most critical factor for influencing evaporation reduction. A straightforward linear relationship can be inferred between evaporation reduction and OCR, with coefficients of 0.58 for configuration *I* and 0.43 for configuration *II*. This correlation provides a clear and practical guideline for optimising FPV designs.

Other design choices, such as dividing the plant into multiple islands or its positioning within the reservoir, have a negligible impact on evaporation reduction.

However evaporation reduction remains influenced by atmospheric conditions, which are out of our control, particularly the wind orientation and velocity. Depending on wind orientation, the effectiveness of the FPV plant can vary significantly. For example, with FPV panels oriented to the south (as is common in the Southern Hemisphere), when winds come from the north, excessive turbulence generated by the panel angle reduces the plant's efficiency to just 4% with an OCR of 50%. In contrast, with crosswinds, the evaporation reduction reaches 26.5%. Moreover, lower wind speeds tend to enhance the reduction in evaporation, while other atmospheric factors like relative humidity and water temperature have little impact, indicating that FPV systems can perform effectively across diverse climates.

Ultimately, this study underscores the dual potential of FPV systems: not only as a key player in renewable energy production but also as an innovative solution for water resource conservation. The ability of FPV plants to significantly mitigate evaporation positions them as a powerful tool for sustainable resource management, capable of addressing both energy and environmental challenges.

Nomenclature

Variables

β	Mass transfer coefficient
ε_{evap}	Evaporation reduction
q	Specific humidity
E	Evaporation rate
ρ	Moist density
v_t	Turbulent viscosity
u^*	Friction velocity
Z_0	Roughness length
T	Temperature
RH	Relative humidity

Constants

κ	Von Kármán Constant
S_{c_t}	Turbulent Schmidt number
$C_{p,v}$	Specific heat capacity of moist air
g_z	Vertical component of the gravity

Subscripts and superscripts

CFD	Computational fluid dynamics
FPV	Floating photovoltaics
PV	Photovoltaics
OCR	Overall Coverage Ratio
GCR	Ground Coverage Ratio
WCR	Water Coverage Ratio
MOST	Monin-Obukhov Similarity Theory
RANS	Reynolds-Averaged Navier-Stokes
CFL	Courant–Friedrichs–Lewy

Geometry

S_{FPV}	FPV power plant surface
S_{Lake}	Lake surface
S_{PV_w}	FPV surface in direct contact with water
S_{PV}	PV panels surface

Funding

ANRT/EDF-CIFRE contract grant/award number: 2023-0411.

Conflicts of interest

The authors have nothing to disclose.

Data availability statement

The data that support the findings of this study are available from the corresponding author upon reasonable request.

Author contribution statement

All the authors were involved in the preparation of the manuscript. All the authors have read and approved the final manuscript.

References

1. A. Sahu, N. Yadav, K. Sudhakar, Floating photovoltaic power plant: a review, Renew. Sustain. Energy Rev. **66**, 815 (2016)
2. H. Liu, V. Krishna, J.L. Leung, T. Reindl, L. Zhao, Field experience and performance analysis of floating pv technologies in the tropics, Prog. Photovolt.: Res. Appl. **26**, 957 (2018)
3. K. Trapani, M.R. Santafé, A review of floating photovoltaic installations: 2007-2013, Prog. Photovolt.: Res. Appl. **23**, 524 (2015)
4. Z. Dobrotkova, Where Sun Meets Water: Floating Solar Handbook for Practitioners. Technical report (World Bank Group, Washington, D.C, 2019)
5. M. Dörenkämper, A. Wahed, A. Kumar, M. de Jong, J. Kroon, T. Reindl, The cooling effect of floating pv in two different climate zones: a comparison of field test data from the netherlands and singapore, Sol. Energy **219**, 15 (2021)

6. L. Micheli, The temperature of floating photovoltaics: case studies, models and recent findings, Sol. Energy **242**, 234 (2022)
7. M.E. Taboada, L. Cáceres, T.A. Graber, H.R. Galleguillos, L. F. Cabeza, R. Rojas, Solar water heating system and photovoltaic floating cover to reduce evaporation: experimental results and modeling, Renew. Energy **105**, 601 (2017)
8. M. Redón-Santafé, P.-S. Ferrer-Gisbert, F.-J. Sánchez-Romero, J.B. Torregrosa Soler, J.J. Ferrán Gozálvez, C.M. Ferrer Gisbert, Implementation of a photovoltaic floating cover for irrigation reservoirs, J. Clean. Prod. **66**, 68 (2014)
9. M. Kumar, A. Kumar, Performance assessment of different photovoltaic technologies for canal-top and reservoir applications in subtropical humid climate, IEEE J. Photovolt. **9**, 722 (2019)
10. M. Al-Widyan, M. Khasawneh, M. Abu-Dalo, Potential of floating photovoltaic technology and their effects on energy output, water quality and supply in Jordan, Energies **14**, 8417 (2021)
11. M.P. Campos Lopes, S. de Andrade Neto, D.A. Castelo Branco, M.A.V. de Freitas, N. da Silva Fidelis, Water-energy nexus: floating photovoltaic systems promoting water security and energy generation in the semiarid region of Brazil, J. Clean. Prod. **273**, 122010 (2020)
12. S. Assouline, K. Narkis, D. Or, Evaporation from partially covered water surfaces, Water Resour. Res. **46**, 1 (2010)
13. U. Stiubiener, A.G. de Freitas, J. Heilala, I. Fuser, PV to reduce evaporative losses in the channels of the São Francisco's river water transposition project, Sci. Rep. **14**, 6741 (2024)
14. F.B. Scavo, G.M. Tina, A. Gagliano, S. Nižetić, An assessment study of evaporation rate models on a water basin with floating photovoltaic plants, Int. J. Energy Res. **45**, 167 (2021)
15. D. Mittal, B.K. Saxena, K.V.S. Rao, Comparison of floating photovoltaic plant with solar photovoltaic plant for energy generation at jodhpur in India, in *2017 International Conference on Technological Advancements in Power and Energy* (*TAP Energy*) (2017), pp. 1–6
16. D. Mittal, B.K. Saxena, K.V.S. Rao, Potential of floating photovoltaic system for energy generation and reduction of water evaporation at four different lakes in Rajasthan, in *2017 International Conference On Smart Technologies For Smart Nation (SmartTechCon)* (IEEE, 2017), pp. 238
17. M. Rosa-Clot, G.M. Tina, S. Nizetic, Floating photovoltaic plants and wastewater basins: an australian project, Energy Proc. **134**, 664 (2017)
18. D.L. McJannet, I.T. Webster, M.P. Stenson, B.S. Sherman, *Estimating open water evaporation for the Murray-Darling basin: a report to the Australian government from the CSIRO Murray-Darling basin sustainable yields project* (CSIRO, Melbourne, 2008), Vol. 50
19. F.R. dos Santos, G.K. Wiecheteck, J.S. das Virgens Filho, G. A. Carranza, T. Lynn Chambers, A. Fekih, Effects of a floating photovoltaic system on the water evaporation rate in the passaúna reservoir, Brazil, Energies **15**, 6274 (2022)
20. F. Archambeau, N. Méchitoua, M. Sakiz, Code_Saturne: a finite volume code for the computation of turbulent incompressible flows − industrial applications, Int. J. Finite Vol. **1**, 1 (2004)
21. A.S. Monin, A.M. Obukhov, Basic laws of turbulent mixing in the surface layer of the atmosphere, Tr. Akad. Nauk. SSSR Geophiz. Inst. **24**, 163 (1954)
22. M.Z. Jacobson, *Fundamentals of Atmospheric Modeling* (Cambridge University Press, Cambridge, UK, 1999)
23. J.-F. Wald, Lois de paroi adaptatives pour un modèle de fermeture du second ordre dans un contexte industriel, PhD thesis, Université de Pau et des Pays de l'Adour (2016)
24. B. Amiot, Modélisation et optimisation du productible de centrales photovoltaiques flottantes, PhD thesis, Université Claude Bernard-Lyon I (2023)
25. D.J. Glanz, G.T. Orlob, Lincoln Lake ecologic study, Water Resour. Eng. DACW27-73-C-0064 (1973)
26. H. Charnock, Wind stress on a water surface, Quart. J. Royal Meteorolog. Soc. **81**, 639 (1955)
27. E.F. Bradley, A micrometeorological study of velocity profiles and surface drag in the region modified by a change in surface roughness, Quart. J. Royal Meteorolog. Soc. **94**, 361 (1968)
28. K. Ilgen, D. Schindler, S. Wieland, J. Lange, The impact of floating photovoltaic power plants on lake water temperature and stratification, Sci. Rep. **13**, 7932 (2023)
29. Q. Abdelal, Floating pv; an assessment of water quality and evaporation reduction in semi-arid regions, Int. J. Low-Carbon Technol. **16**, 732 (2021)
30. M.R. Hipsey, L.C. Bruce, C. Boon, B. Busch, C.C. Carey, D. P. Hamilton, P.C. Hanson, J.S. Read, E. De Sousa, M. Weber et al., A general lake model (GLM 3.0) for linking with high-frequency sensor data from the global lake ecological observatory network (GLEON), Geosci. Model Develop. **12**, 473 (2019)
31. K. Ilgen, D. Schindler, A. Armbruster, R. Ladwig, I.E. Ruiz de Zarate, J. Lange, Evaporation reduction and energy generation potential using floating photovoltaic power plants on the aswan high dam reservoir, Hydrol. Sci. J. **69**, 1 (2024)

Cite this article as: Baptiste Berlioux , Baptiste Amiot, Martin Ferrand, Rémi Le Berre, Oume-Lgheit Rhazi, Javier Vidal, Hervé Pabiou, Ronnie Knikker, Numerical analysis of evaporation reduction in floating photovoltaic power plants: influence of design parameters, EPJ Photovoltaics **16**, 4 (2025)